Ionization dynamics in fast ion-atom collisions. II. Final-state momentum distributions of the ionization products in collisions of He with bare carbon ions

Lokesh C. Tribedi,[1,*] P. Richard,[2] Y. D. Wang,[2] C. D. Lin,[2] R. E. Olson,[3] and L. Gulyas[4]
[1]*Tata Institute of Fundamental Research, Homi Bhabha Road, Colaba, Mumbai-400005, India*
[2]*J. R. Macdonald Laboratory, Department of Physics, Kansas State University, Manhattan, Kansas 66506-2601*
[3]*Physics Department, University of Missouri–Rolla, Rolla, Missouri 65401*
[4]*Institute of Nuclear Research of the Hungarian Academy of Science (ATOMKI), P.O. Box 51, H-4001 Debrecen, Hungary*
(Received 20 April 1998)

We have used the energy and angular distributions of the low-energy electron emission cross sections from the preceding paper [Lokesh C. Tribedi *et al.*, Phys. Rev. A **58**, 3619 (1998)] to derive the doubly differential final-state longitudinal momentum distributions of the electrons, recoil ions, and projectiles in ion-atom ionization for C^{6+}+He. The complementary nature of the electron spectroscopy and the recoil-ion momentum spectroscopy have been investigated using a formulation based on three-body kinematics to explore the ionization dynamics in detail. The influence of the three-body ionization as well as the binary-encounter processes on the recoil-ion (and projectile) longitudinal momentum distributions has been investigated. The separation of the soft- and hard-collision branches of recoil-ion distributions is an important feature of the present technique. The present method also allows one to determine cross sections for very large electron momenta. The single-differential distributions are also derived by numerical integration of the double-differential distributions. The first Born approximation, the continuum distorted wave eikonal initial state, and the classical trajectory Monte Carlo calculations are used to explain the data.
[S1050-2947(98)04910-5]

PACS number(s): 34.50.Fa, 39.30.+w, 34.10.+x

I. INTRODUCTION

The energy and angular distributions of the low-energy electrons measured by standard electron spectroscopic techniques have enriched our understanding regarding the ion-atom ionization mechanisms. The distinct features characterizing the ionization process are the soft-collision, the electron capture in a continuum (ECC) cusp, and the binary-encounter peak. The low-energy electrons produced in the soft collisions largely dominate the double-differential ionization cross-section spectrum. These soft electrons can be viewed as a continuation of excitation across the ionization threshold. The cusp electrons observed at 0° are produced by electron capture to the continuum and are identified as a cusplike structure at an electron velocity that matches the projectile velocity. The broad peak is of binary-encounter electrons that are elastically scattered target electrons from the projectile nucleus and centered around an electron velocity that is twice the projectile velocity. The high-resolution Auger electron spectroscopy has been used to study various phenomena in ion-atom ionization such as resonant transfer and excitation, inelastic resonant excitation, and electron-electron interactions [1–3]. The energy and angular distributions of the low-energy electrons in ion-atom collisions have provided important inputs in understanding the two-center mechanism of ionization (see references in the preceding paper, henceforth referred to as paper I).

While electron spectroscopy has been used extensively to study the ionization mechanism, the use of recoil-ion momentum spectroscopy (RIMS) is relatively new. Longitudinal recoil-ion momentum spectroscopy is an experimental technique that has been developed only in the past few years [4–12]. This method offers a very powerful technique to study ion-atom collisions different from the conventional approaches. The high-resolution RIMS technique has enriched our understanding regarding the different inelastic processes such as ionization and capture. The separation of the electron-electron interaction from the nuclear-electron interaction in ion-atom ionization has been investigated using this technique [11,12]. Kinematically complete experiments on single ionization [6], double ionization [8], and transfer ionization [7] have been carried out recently using RIMS via the measurements of the differential cross sections in the recoil ion (p_R) and electron momenta (p_e). Most of these kinematically complete experiments typically use a cold jet target [9] of He gas. The single differential cross sections ($d\sigma/dp_{R\|}$ and $d\sigma/dp_{e\|}$) are measured, which involves the detection of recoil ions in coincidence with soft electrons (and projectiles) having energies below 50 eV. Recently, Kravis *et al.* [10] also have studied the details of the ejected electron momentum distributions in ionization of He by low-velocity protons and C^{6+} ions.

Both ejected electron spectroscopy (EES) and RIMS have been used to investigate various phenomena of ion-atom collisions. However, the relationships and complementary nature of these two techniques have not been explored in detail. It has been demonstrated only recently [13,14] that many of the aspects that are studied using the RIMS also can be addressed by EES, although the latter is not a kinematically complete experiment. The standard electron spectroscopy experiment has the added advantage in that it does not need a cold jet target. Since the spread in the electron energy due to

*Electronic address: lokesh@tifrc3.tifr.res.in

the thermal energy of the He atom is of the order of 0.005 meV, i.e., the momentum spread is approximately equal to 6×10^{-4} a.u., we can derive the electron momenta without the use of a cold jet target. The disadvantages of the EES method are that the charge state of the recoil ion is not resolved and the recoil ion and projectile momenta cannot be deduced for the transverse direction. In this paper we show that from the measured energy and angular distributions of the lowest-energy electrons, with a double differential cross section (DDCS) $(d^2\sigma/d\varepsilon_e d\Omega_e)$, one can derive a variety of double-differential distributions by using three-body kinematics (ε_e and Ω_e are the electron energy and emission solid angle). The final-state momentum distributions of the electron, the recoil ion, and the projectile in ion-atom ionization contain rich information regarding the three-body dynamics that has important applications in other branches of physics. For example, we have derived differential cross sections in the longitudinal momentum distributions of the recoil ions $d^2\sigma/dp_{R\|}d\Omega_e$ and projectiles $d^2\sigma/dp_{P\|}d\Omega_e$. For the electrons we derive the complete momentum distributions, i.e., longitudinal and transverse components $d^2\sigma/dp_{e\|}d\Omega_e$ and $d^2\sigma/dp_{e\perp}d\Omega_e$. By integrating these distributions over θ_e (i.e., the electron emission angle) we can obtain the single-differential distributions in terms of the momentum transferred to all three particles, i.e., $d\sigma/dp_{R\|}$, $d\sigma/dp_{e\|}$, and $d\sigma/dp_{P\|}$, which are the foci of a recent series of RIMS experiments on ionization. The quantity $p_{e\perp}$ is the electron transverse momentum.

It has been demonstrated [6] that these single-differential distributions are sensitive to the postcollision interaction between the ionized electron and the projectile for highly charged heavy projectiles. The peak shifts of the longitudinal momentum distributions of the electrons towards positive momentum and that of the recoil ions towards negative momentum have been reproduced extremely well for $Ni^{24+}+He$ by classical trajectory Monte Carlo (CTMC) calculations. However, the peak shifts observed in experiments were in large disagreement with the predictions of continuum distorted wave eikonal initial-state (CDW-EIS) calculations [15]. In the present paper, we study the momentum distributions for a high-velocity ($v=10$ a.u.) collision of $C^{6+}+He$ for which the postcollision effect is expected to be smaller than that for the collision system in Ref. [6] since the current perturbation strength $Z/v=0.6$, rather than 2.0 for the Ni^{24+} system. We compare our data with the CDW-EIS, first Born (B1) and CTMC calculations.

II. RESULTS AND DISCUSSION

A. Relation between the longitudinal momentum of the electrons and the recoil ions

The connection between the longitudinal recoil-ion momentum distributions and ejected electron spectroscopy was recently discussed by Rodríguez *et al.* [16]. These authors have analyzed the ionization mechanisms from the perspective of longitudinal recoil-ion momentum distributions. In this paper our objective is to show how we can construct momentum distributions for the projectile and recoil ions based on the electron DDCS measurements. For fast ion-atom collisions, longitudinal momentum and energy conservation require that

$$-p_{P\|}=p_{e\|}+p_{R\|}=Q/v=(\varepsilon_e-\varepsilon_i)/v, \tag{1}$$

where $p_{P\|}$ is the longitudinal momentum transfer from the projectile, $p_{e\|}\,(=p_e\cos\theta_e)$ is the longitudinal electron momentum, $p_{R\|}$ is the longitudinal recoil-ion momentum, $|\varepsilon_i|$ is the binding energy of the target atom in the initial state, and ε_e is the ejected electron energy. This relation is valid if the projectile scattering angle is very small. In other words, Eq. (1) is a good approximation for a three-body system involving a heavy projectile that suffers a small energy loss compared to its initial energy and is correct to the order of m_e/m_P and m_e/m_T, where m_e, m_P, m_T represent the mass of the electron, projectile, and target, respectively. The recoil ions can be uniquely defined only in collisions of bare ions with atomic hydrogen. In the case of other targets (such as H_2/He) the recoil ions also can be produced from double or dissociative ionization and in such cases Eq. (1) merely reflects the momentum balance in the center-of-mass frame of the ''compound'' third party that is separable from the ionized electron and the projectile. For the present collision system ($C^{6+}+He$) the cross section for double ionization is estimated to be about 5% of the total ionization cross section. This estimation is based on the present CTMC calculation and previous experiments [17–19]. Therefore, it is reasonable to assume that the most probable recoil ion would be He^+ in the present case. However, this assumption becomes more tenuous for the small-impact-parameter collisions that lead to backward scattered electrons and the fraction of double ionization probability (with respect to single ionization) will then be greater than its integrated value. The He^+ can also be left excited. This channel is not separated from the He^+ ground-state channel in the present experiment.

The longitudinal recoil-ion momentum ($p_{R\|}$) can be determined from Eq. (1) for a given electron energy and emission angle (ε_e, θ_e). In general, for a given $p_{R\|}$, there are two branches of electron energy

$$\begin{aligned}\varepsilon_e(p_{R\|},\theta_e)&=\varepsilon_e^{\pm}\\&=[p_{R\|}v-|\varepsilon_i|+(v\cos\theta_e)^2]\\&\quad\pm|v\cos\theta_e|\sqrt{(v\cos\theta_e)^2+2(p_{R\|}v-|\varepsilon_i|)}.\end{aligned} \tag{2}$$

It may be noted that for $p_{R\|}<p_{R\|}^0=|\varepsilon_i|/v$, $\varepsilon_e(p_{R\|},\theta_e)$ is a double-valued function of $p_{R\|}$ for a given θ_e. The quantity $p_{R\|}^0$ corresponds to zero-energy electrons as explained in Eq. (1). For $p_{R\|}=0$ and $\theta_e=0°$ the solution (2) gives $p_e=v\pm\sqrt{v^2-2|\varepsilon_i|}$, which, for $\varepsilon_i\approx0$, can be further simplified to give $p_e\approx2v$ and 0. The first solution implies the binary encounter process, while the second solution corresponds to very-low-energy electron emission in a large-impact-parameter collision, resulting in very small recoil-ion momentum in a three-body ionization.

Rodríguez *et al.* [16] pointed out that the two energy branches corresponding to the electron energies ε_e^+ and ε_e^- join together at electron capture into the projectile continuum $\varepsilon_e^+=\varepsilon_e^-=\frac{1}{2}v^2$ since $\theta_e=0$ and $p_e=v$. The longitudinal recoil-ion momentum acquires an absolute minimum at the ECC, $p_{R\|}^{\min}=-v/2+|\varepsilon_i|/v$, marking the threshold of the longitudinal recoil-ion momentum distribution.

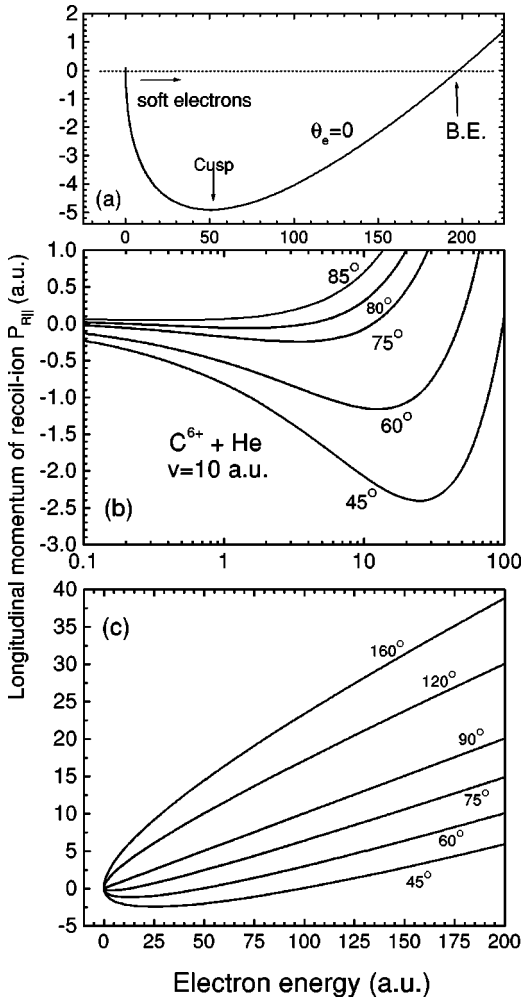

FIG. 1. Relation between the longitudinal momentum of the recoil ions ($p_{R\|}$) and the electron energy (ε_e) for (a) $\theta_e=0°$, (b) forward angles, and (c) forward and backward angles in ionization of He by 30-MeV C^{6+}ions, obtained from Eqs. (1) and (2).

Figure 1 shows the relation between the recoil-ion longitudinal momentum and the electron energy for a given emission angle for the present collision system. It is clearly seen that for $\theta_e<90°$ two different values of ε_e can have the same longitudinal momentum of the recoil ions. For backward angles the $p_R\|$ becomes a single-valued function of ε_e. It may be seen from Fig. 1(a) that for 0° electron emission the zero recoil-ion longitudinal momentum ($p_{R\|}$) is observed for $\varepsilon_e=0$, i.e., for the soft-collision electrons (SCEs) and $\varepsilon_e \cong 200$ a.u., which is the binary-encounter (BE) electron energy for the present case since $v=10$ a.u. The $p_{R\|}$ is expected to be near zero at the BE since it is a two-body collision between the electron and the projectile (we have assumed that the shift in the binary peak due to the electrons initial binding energy is negligible for this illustration). The curve turns over at the cusp electron energy $t=50$ a.u. for 0°. For all the forward angles $p_R\|(\varepsilon_e,\theta_e)$ becomes zero twice, once for SCEs and once for BE electrons. Since the BE peak energy ($\varepsilon_{\mathrm{BE}}=4t\cos^2\theta_e$) becomes smaller for higher emission angles, the turnover point gradually shifts [Figs. 1(b) and 1(c)] towards low electron energies for higher emission angles. The curve $p_R\|(\varepsilon_e,\theta_e)$ becomes a monotonically increasing single-valued function of ε_e for $\theta_e \geqslant 90°$ [Fig. 1(c)] and no binary encounter peak is observed for back angles.

B. Double differential distributions

The final-state electron longitudinal and transverse momentum distributions in terms of electron DDCSs can be expressed as

$$\frac{d^2\sigma}{dp_{e\|}d\Omega_e}=\frac{|p_{e\|}|}{\cos^2\theta_e}\frac{d^2\sigma}{d\varepsilon_e d\Omega_e} \tag{3}$$

and

$$\frac{d^2\sigma}{dp_{et}d\Omega_e}=\frac{|p_{e\perp}|}{\sin^2\theta_e}\frac{d^2\sigma}{d\varepsilon_e d\Omega_e}. \tag{4}$$

Equation (1) provides the essential ingredients for constructing longitudinal momentum distributions for the recoil ions and for the projectiles in the final state. Having obtained the longitudinal recoil-ion momentum, we can calculate $d^2\sigma/dp_{R\|}d\Omega_e$ from the following equation, using the Jacobian transformation:

$$\frac{d^2\sigma}{dp_{R\|}d\Omega_e}=\left|\frac{1}{\frac{1}{v}-\frac{\cos\theta_e}{\sqrt{2\varepsilon_e}}}\right|\frac{d^2\sigma}{d\varepsilon_e d\Omega_e}. \tag{5}$$

In Fig. 2 we show a few examples of the longitudinal momentum distributions of the electrons and recoil ions (corresponding to the electrons having energies 0.1–300 eV). For forward angles, the electron longitudinal momentum distribution peaks at some positive $p_{e\|}$, as expected. The peak of the distribution corresponds to the low-energy electrons emitted in three-body ionization. For $\theta_e=45°$ the measured electron distribution shows both peaks corresponding to the soft electrons (around 0.5 a.u.) as well as to the binary-encounter peak (around 10 a.u.). Accordingly, the recoil-ion distributions for the forward (electron emission) angles peak at negative $p_{R\|}$ values, as can be predicted from Eq. (1). The two branches of the recoil-ion distributions are clearly visible. The higher branch corresponds to the low-energy electrons produced in three-body soft collisions (soft electrons). An example is shown in Fig. 2(b) for emission angle 45°. The higher branch peaks around $p_{R\|}\approx -0.45$ a.u., which has a corresponding electron counterpart at $p_{e\|}\approx 0.57$. These peaks (both recoil and electron) originate from the lowest-energy part (below approximately 10 eV) of the electron DDCS spectrum. Hence the detection of these low-energy electrons is important in order to have the complete peak in the recoil-ion momentum distribution. It may be noticed that the lower branch has a broad peak around $p_{R\|}\approx 0.0$, which corresponds to the binary encounter peak in the electron spectrum. Since this peak essentially is produced in a two-body collision between the electrons and the projectiles, the recoil ions are not expected to have any momentum (i.e., $p_{R\|}\approx 0.0$) at the peak of the distributions. The width of the distribution arises due to the Compton profile of the target nucleus since in the center-of-mass frame of the target system the nucleus has the same Compton profile as the elec-

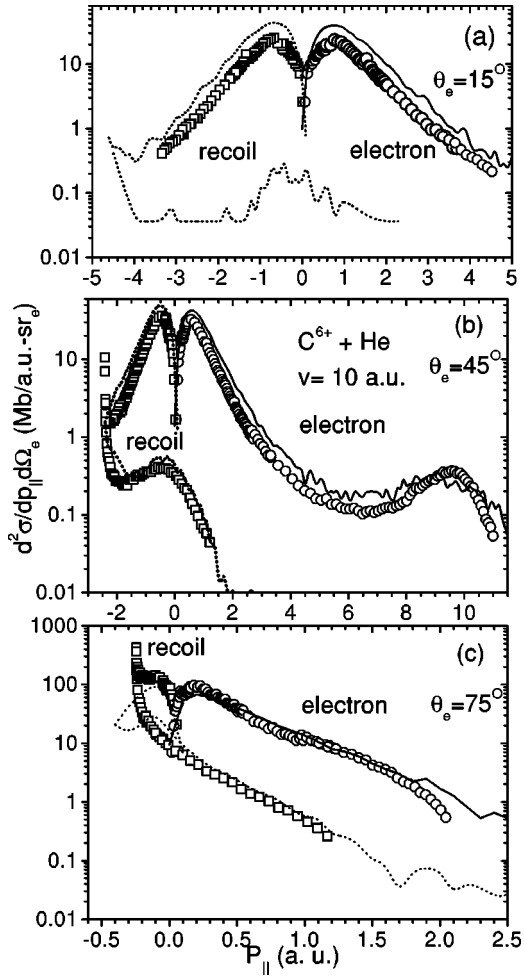

FIG. 2. Double differential longitudinal momentum distributions of electrons (open circles) and recoil ions (open squares) for forward angles; (a) $\theta_e = 15°$, (b) $\theta_e = 45°$, and (c) $\theta_e = 75°$. The thick solid (dotted) line is the CTMC calculation for electron (recoil) distributions.

tron. As in the electron DDCS spectrum, the soft electrons, i.e., the upper branch, contribute the most to the total ionization cross section. In fact, the cross sections for the recoil ions produced in the binary encounter, i.e., in the lower branch, are two to three orders of magnitude smaller compared to the upper branch. In conventional RIMS measurements, the measured single-differential ($d\sigma/d\Omega_e$) recoil-ion distributions are composed of the contributions of the recoil ions from both branches, but is dominated by the upper branch. Using the present method we are able to distinguish clearly the separate contributions of the three-body collision and the binary-encounter mechanisms of the recoil-ion production. The two branches join together at the threshold value of recoil longitudinal momentum ($p_{R\|}^{\min}$) at which the cross section goes through a singularity. This can be seen from Eq. (5). The right-hand side of this equation has a divergence for $p_e = v \cos\theta_e$. This divergence could arise due only to the mathematical transformation and may not have any physical basis. However, this sharp divergence separates clearly the two branches that correspond to the soft-collision (''soft-branch'') and hard-collision (''hard-branch'') regimes of ionization. It may be emphasized here that the present method allows one to determine the cross sections of electrons and projectiles with very high momenta that are not easily achieved in RIMS.

In order to understand these distributions we have performed CTMC calculations for the present collision system. The electron double-differential cross sections have already been compared in detail with the CDW-EIS and B1 calculations in paper I. Therefore, the electron and recoil-ion momentum distributions are not compared with the CDW-EIS or the B1 calculations since these calculations also use the same transformations as used above. The CTMC calculation, on the other hand, is a complete three-body calculation and does not require any such transformation and hence can provide an independent check on the method we have used to transform the experimental data. Along with the three-body calculations, the four-body CTMC calculations were also used to determine the contributions from double ionization of He. The three-body and four-body calculations give the same peak shapes and almost the same magnitude. It was found that the total electron spectra contain a 5% contribution from the double ionization at small angles, increasing to about 15% for the largest backward angle studied. In Figs. 2(a), 2(b), and 2(c) we show such comparisons with the data for $\theta_e = 15°$, 45°, and 75°, respectively. It may be noted that the two branches in the recoil-ion distributions are reproduced in these calculations and in general the qualitative agreement is very good. The two branches could be reproduced by the CTMC calculations after identifying the collisions producing low- and high-energy ($\varepsilon_e \gtrless \frac{1}{2}v^2\cos^2\theta_e$) electrons. This was achieved by introducing coincidence conditions on the recoil ions and electrons in the CTMC calculation. The observation of two branches in the recoil-ion longitudinal momentum distribution and its independent check by the CTMC calculations is an important feature of the present technique. For small angles such as 15° the calculations overestimate the observed data for electrons and recoils. However, for higher angles ($15° \leqslant \theta_e \leqslant 90°$) the agreement is much better. The CTMC calculation predicts the distributions extremely well for $\theta = 75°$. In the case of backward angles (Fig. 3) the electrons peak at a negative longitudinal momentum and accordingly the recoil-ion distributions at a positive momentum. The agreement between the theory and the data is good only for $p_{R\|} \geqslant 1$ a.u. and $p_{e\|} \leqslant 1$ a.u. The agreement with the theory at the soft-electron peak is poor for large backward angles. The CTMC calculation shows that the double ionization could be approximately 15% (amounting to 30% electron yields) of the single ionization for the large backward angles. However, the discrepancy between the theory and experiment is too large to be explained by the double ionization contribution. Such doubly differential measurements can be carried out by detecting the recoil ions in coincidence with the ejected electrons emitted in a given direction, using a cold jet target. No such measurements have been reported.

The projectile momentum transfer distribution can be given by

$$\frac{d^2\sigma}{dp_{P\|}d\Omega_e} = v\,\frac{d^2\sigma}{d\varepsilon_e d\Omega_e}. \tag{6}$$

These distributions are shown in Fig. 4 for a few different

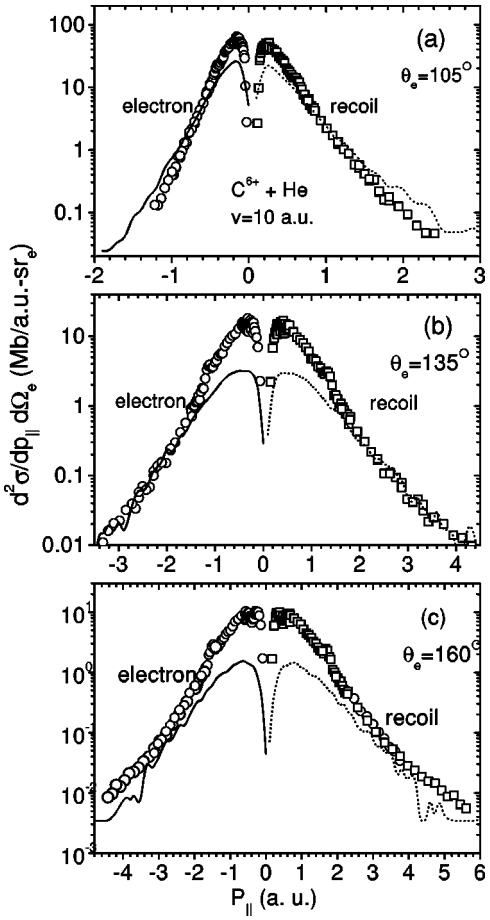

FIG. 3. Same as in Fig. 2 except for backward angles; (a) $\theta_e = 105°$, (b) $\theta_e = 135°$, and (c) $\theta_e = 160°$. The lines and symbols have same meaning as in Fig. 2.

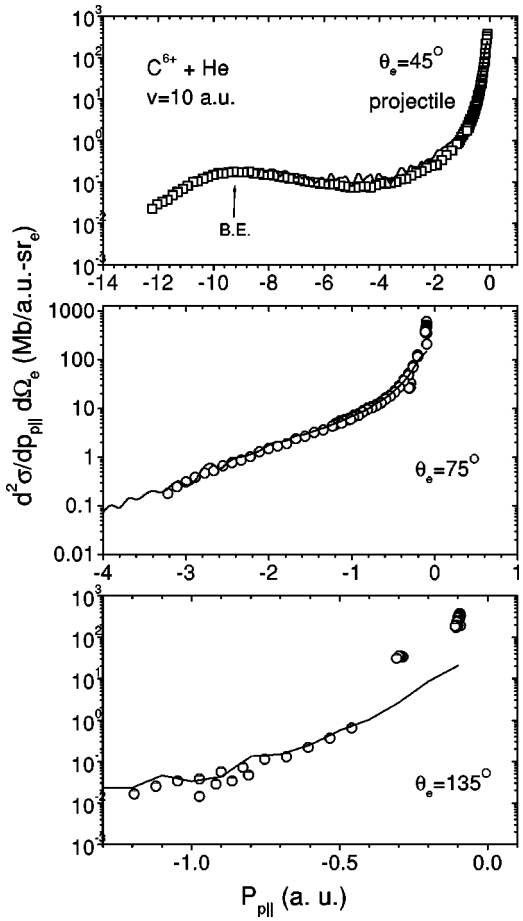

FIG. 4. Double-differential distributions of projectile longitudinal momentum transfer for (a) $\theta_e = 45°$, (b) $\theta_e = 75°$, and $\theta_e = 135°$. The line represents the CTMC calculations.

angles. The minimum energy loss of a projectile to ionize a He atom is 0.903 a.u., which corresponds to a minimum momentum transfer $p^0_{P\|} = -0.0903$ a.u. (since $v = 10$ a.u.) of the projectile. Accordingly, the projectile longitudinal momentum transfer distribution starts at -0.0903 a.u. and falls off rapidly. The binary encounter peak is clearly observed as a broad peak around -10 a.u. The double-differential distributions are well reproduced by the CTMC calculations for the forward angles [Figs. 4(a) and 4(b)]. The soft-electron peak contributes the most in the projectile momentum distribution. However, for backward angles the CTMC underestimates the distributions for very small momentum transfer but agrees very well for large momentum transfer. The double-differential distributions in electron energy and projectile scattering angle have been measured recently [20] for low-energy protons colliding with He. A postcollision interaction was observed by these authors.

The electron transverse momentum distributions for different emission angles [derived using Eq. (4)] are shown in Fig. 5. The transverse momentum of the ionization products is sensitive to the impact parameter. In the present case the distributions show a peak around 0.3–0.5 a.u. for different angles. These peaks correspond to the soft-electron peaks. For $\theta_e = 45°$ the binary-encounter peak is clearly visible around $p_{e\perp} = 10$ a.u., as expected from the kinematics. At the BE peak, since the recoil momentum is near zero, the transverse momentum exchange between the projectile and the electron is dominant and the projectile transverse momentum would be the same in magnitude as the electron transverse momentum ($p_{e\perp}$), i.e., approximately equal to 10 a.u., which corresponds to a scattering angle $p_{e\perp}/p_P$ about 0.01 mrad. The CTMC calculations reproduce the distributions very well for large forward angles [Figs. 5(b) and 5(c)]. Excellent agreement is observed for 75°. For the small forward angle [Fig. 5(a)] the theory overestimates the distribution for all the transverse momentum. For large backward angles [Fig. 5(d)] the theory underestimates the data for low-momentum values.

III. SINGLE-DIFFERENTIAL DISTRIBUTIONS

Single-differential distributions such as $d\sigma/dp_{R\|}$, $d\sigma/dp_{e\|}$, $d\sigma/dp_{P\|}$ have been derived by performing numerical integration of the corresponding double-differential distributions at different angles between 15° and 160°. We show the longitudinal momentum distributions of the electrons and recoil ions in Fig. 6(a). It may be seen that the electron distribution is slightly shifted towards a positive longitudinal momentum by 0.1 a.u. (which is approximately the same as Q/v of the reaction for zero-energy electrons). The recoil-ion longitudinal momentum distribution peaks between 0 and -0.1 a.u. Since the forward shift of the electron distribution can be accounted for almost fully by the projectile energy loss for the emission of lowest-energy electrons,

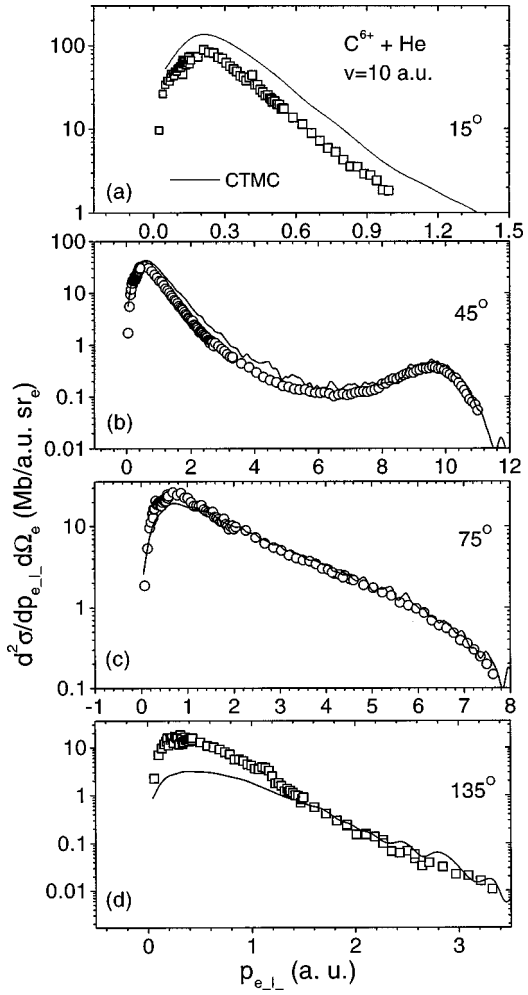

FIG. 5. Double-differential transverse momentum distributions of electrons for different electron emission angles; (a) $\theta_e = 15°$, (b) $\theta_e = 45°$, (c) $\theta_e = 75°$, and (d) $\theta_e = 135°$. The CTMC calculations are shown by solid lines.

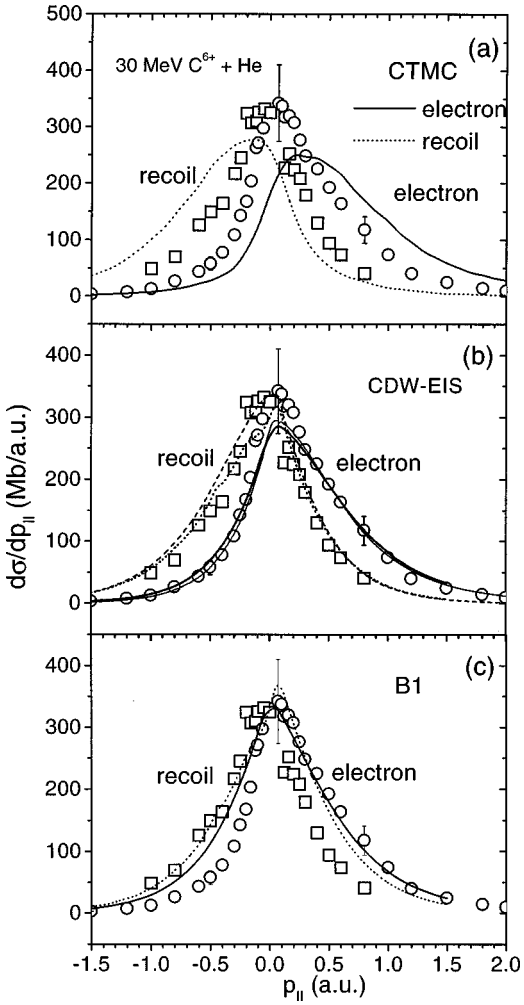

FIG. 6. Single-differential longitudinal momentum distributions of electrons (open circles) and recoil ions (open squares) along with different theoretical calculations. (a) The thick solid (dotted) line is the CTMC calculation for electron (recoil) distributions. (b) The thick (thin) solid line represents the CDW-EIS calculation for the electron distribution using HFS (H-like) wave function of the active electron. The dotted (dashed) line denotes the CDW-EIS calculation for the recoil-ion distribution HFS (H-like) wave function. (c) A comparison with the B1 calculations.

it may be concluded that the PCI causes a much smaller shift with respect to that observed in the case of Ni ions [6]. This is consistent with the fact that we have in the present case a much smaller value of Z/v $(=0.6)$ and the PCI is expected to increase with increasing Z/v. The CTMC calculations predict a much larger shift for the electrons as well as for the recoil ions. The observed widths of the distributions are smaller than those given by the CTMC calculations. The overall agreement would be better if one added a 5–10 % contribution due to double ionization in the calculations. However, the CDW-EIS calculations, shown in Fig. 6(b), provide much better agreement with the data. The thin solid line (representing the electron distribution) and the dashed line (corresponding to the recoil-ion distributions) are the CDW-EIS calculations using the H-like wave function of the active electron in the initial state. The thick solid line and dotted line represent the CDW-EIS calculations for electrons and recoil ions, respectively, using Hartree-Fock-Slater wave functions for the initial and final states for the active electron. Both of the CDW-EIS calculations reproduce the peak position very well for the electron distribution. The agreement is good also for the recoil-ion distribution except for a small discrepancy near the maximum. It may be concluded that the small postcollision interaction that is present in the collision is well reproduced by the CDW-EIS calculations. The B1 calculations are shown in Fig. 6(c). Although they reproduce the data for a positive longitudinal momentum, they fail for electrons with a negative longitudinal momentum. Also, they predict the electron peak around $p_{e\|} = 0.0$. The B1 fails to predict the recoil-ion peak position correctly. The single differential distribution in projectile longitudinal momentum transfer $(d\sigma/dp_{P\|})$ obtained by using a transformation similar to Eq. (6) is shown in Fig. 7. The negative $p_{P\|}$ implies a loss of projectile energy in the collision. It may be noticed that the distribution falls sharply beyond -0.09 a.u., which is the minimum momentum required to be transferred for ionization. The CTMC calculation provides reasonable agreement with the data, while the CDW-EIS calculations show excellent agreement with all the data points.

The single-differential distributions can be compared readily with the recent RIMS measurements. Moshammer

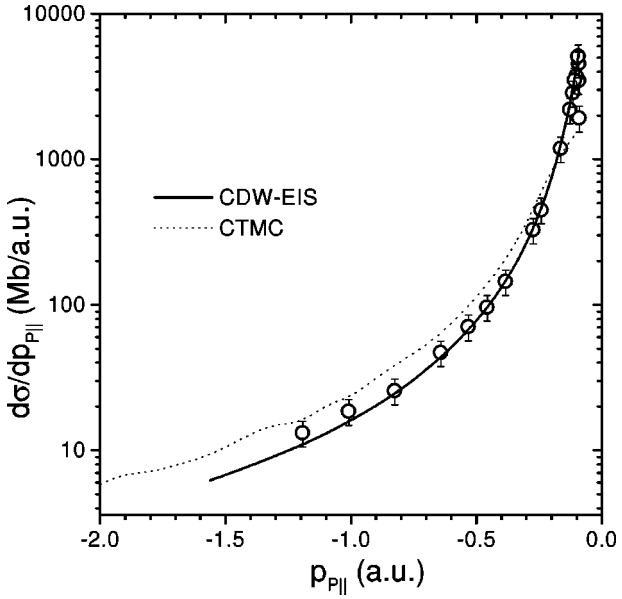

FIG. 7. Single-differential distribution of projectile longitudinal momentum transfer along with the CTMC (dotted line) and CDW-EIS (solid line) calculations.

et al. [6] have measured the recoil-ion and electron single-differential distributions for $Ni^{24+}+He\,(v=12, Z/v\approx 2)$. Their measurements show a large shift in the recoil and electron distributions and these results have been interpreted as a signature of the postcollision interaction between the projectile ions and the ionized electrons since the projectile momentum transfer is negligibly small in this collision. It was also shown that the CTMC calculation reproduces these shifts extremely well. However, the CDW-EIS calculations predict much smaller shifts [15] of the electron and recoil distributions compared to the observation [6], while it reproduces the electron single-differential distribution quite well. Such a discrepancy between the data and CDW-EIS calculation calls for further investigation. It may be interesting to measure the double-differential distributions of the lowest-energy electron emission for a collision system similar to the above one (i.e., 3.6-MeV/nucleon $Ni^{24+}+He$). It may be recalled that in the case of ionization of He by low-velocity ($v\approx 1.0$) highly charged (C^{6+}) ions (nonperturbative regime), both the CDW-EIS and CTMC calculations deviate from the experimental observations [10] regarding the shape of the electron longitudinal momentum distribution.

The single-differential distribution in electron transverse momentum is shown in Fig. 8(a). The distribution peaks around 0.5 a.u. The B1 (dotted line) overestimates the distribution, although it reproduces the peak position quite well. The CTMC calculation (dash-dotted line) predicts the peak position around 0.25 a.u. and the whole distribution is shifted toward lower momentum values. The best agreement is found with the CDW-EIS calculations using the Hartree-Fock-Slater wave function. The CDW-EIS calculation reproduces the peak position as well as the width of the distribution very well. Although there is a discrepancy between the shape of the observed distribution and the CTMC calculations, it reproduces the total ionization cross section within 10% (the theory overestimates it). The width of the distribution is found to be 1 a.u. The width of the longitudinal momentum distribution (Fig. 6) was found to be 0.75 a.u. for electrons as well as recoil ions. These widths are less than that of the Compton profile (1.6 a.u.) of the He target. However, the width of these distributions need not necessarily reflect the Compton profile in the initial state since most of these electrons and recoil ions are produced in the three-body collision and momentum is shared by the recoil ions and the electrons.

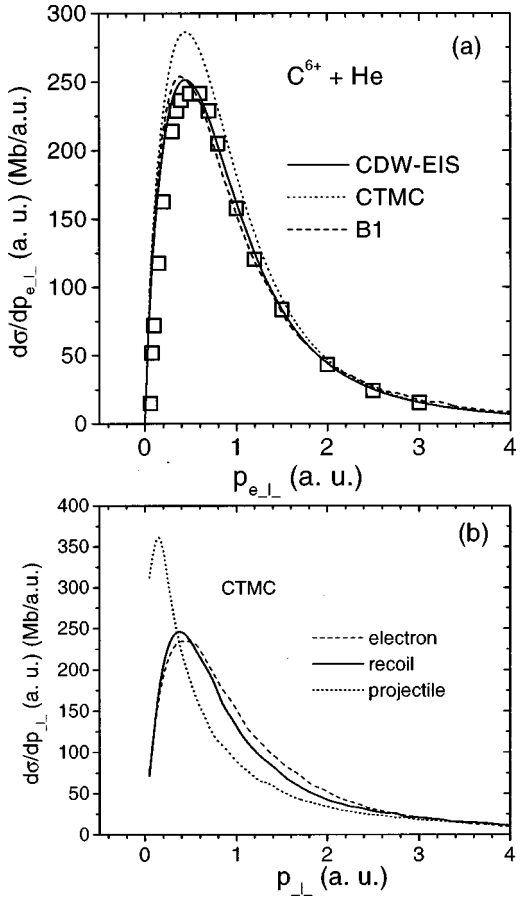

FIG. 8. (a) Single-differential distribution of electron transverse momentum transfer along with the CTMC, CDW-EIS, and B1 calculations. (b) The CTMC calculations for transverse momentum distributions of all three particles.

The transverse momentum of the recoil ions is a result of a complicated interplay among the three particles in the final state. Using the present method it is not possible to derive the transverse momentum distributions of the recoil ions and projectiles from the measured electron spectra since no simple relation among the transverse momenta of the ionization products exists similar to Eq. (1). Extensive measurements on the recoil-ion transverse momentum distribution have been carried out by Dörner *et al.* [21]. However, we show the CTMC calculations for these distributions in Fig. 8(b). Most of the low-energy electron emission is associated with very small projectile transverse momenta (0.1 a.u) and hence for small projectile scattering angles ($p_{P\perp}/p_P\approx 1\times 10^{-4}$ mrad). The soft-electron peak (at 0.2 a.u.) arises from a large impact parameter collision in which the projectile scattering angle is negligibly small and hence the recoil-ion transverse momentum should be almost the same in magnitude as $p_{e\perp}$, as seen from the calculation.

IV. CONCLUSION

We have studied doubly differential longitudinal momentum distributions of the recoil ions and the projectiles in the final state of ion-atom ionization from the measurement of energy and angular distributions of the low-energy electrons for bare carbon ions colliding with He. The details of the ionization kinematics have been worked out based on three-body kinematics. A formulation for constructing these double-differential distributions from the measured electron double-differential distributions is used, based on three-body kinematics. An important feature is the separation of the two branches in the recoil-ion double-differential (in momentum and angle) distribution. The two branches correspond to the three-body soft collision and two-body binary-encounter mechanisms of ionization and they join together through a sharp singularity at the threshold longitudinal momentum. Complete, three-body CTMC calculations reproduce the two branches very well and explain the data for forward angles but underestimate them for backward angles. The single differential longitudinal momentum distributions have been determined for the recoil ions, electrons, and projectiles. We also have derived the electron transverse momentum distribution and it is pointed out that the transverse momentum distributions of the recoil ions and projectiles cannot be investigated using the present technique. The CTMC calculations predict a larger than observed shift in the electron and recoil-ion distributions for the present collision. The CDW-EIS calculations reproduce the data very well along with the electron and recoil peak positions. In view of the fact that the CDW-EIS calculation does not reproduce the earlier observation [6] of a large shift of these distributions caused by strong postcollision interaction, we suggest further investigation of double differential cross sections for the low-energy electron emission from the He atom in a collision with even heavier highly charged projectiles (such as in Ref. [6]). The complementary nature of the electron spectroscopy and the RIMS has been explored in detail and it is shown that many of the aspects of RIMS also can be addressed by the use of conventional electron spectroscopy. The present method does not require a cold jet target and therefore can be used for other targets as well. The present study gives a different direction to the well known EES technique.

ACKNOWLEDGMENTS

The authors would like to thank M. E. Rudd for critically reading this manuscript and for various suggestions. This work was supported by the Division of Chemical Sciences, Office of Basic Energy Sciences, Office of Energy Research, U.S. Department of Energy.

[1] N. Stolterfoht, Phys. Rep. **146**, 315 (1987).
[2] N. Stolterfoht, J. Electron Spectrosc. Relat. Phenom. **67**, 309 (1994).
[3] T. J. M. Zouros, D. H. Lee, and P. Richard, Phys. Rev. Lett. **62**, 2261 (1989).
[4] C. L. Cocke and R. E. Olson, Phys. Rep. **205**, 153 (1991).
[5] R. Ali, V. Frohne, C. L. Cocke, M. Stöckli, S. Cheng, and M. Raphaelian, Phys. Rev. Lett. **69**, 2491 (1992).
[6] R. Moshammer, J. Ullrich, M. Unverzagt, W. Schmidt, P. Jardin, R. E. Olson, R. Mann, R. Dörner, V. Mergel, U. Buck, and H. Schmidt-Böcking, Phys. Rev. Lett. **73**, 3371 (1994).
[7] V. Mergel, R. Dörner, M. Achler, Kh. Khayyat, S. Lencinas, J. Euler, O. Jagutzki, S. Nüttgens, M. Unverzagt, L. Spielberger, W. Wu, R. Ali, J. Ullrich, H. Cederquist, A. Salin, C. J. Wood, R. E. Olson, Dz. Belkić, C. L. Cocke, and H. Schmidt-Böcking, Phys. Rev. Lett. **79**, 387 (1997).
[8] R. Moshammer, J. Ullrich, H. Kollmus, W. Schmitt, M. Unverzagt, O. Jagutzki, V. Mergel, H. Schmidt-Böcking, R. Mann, C. J. Woods, and R. E. Olson, Phys. Rev. Lett. **77**, 1242 (1996).
[9] J. Ullrich, R. Dörner, V. Mergel, O. Jagutzki, L. Spielberger, and H. Schmidt-Böcking, Comments At. Mol. Phys. **30**, 285 (1994).
[10] S. D. Kravis, M. Abdallah, C. L. Cocke, C. D. Lin, M. Stockli, B. Walch, Y. D. Wang, R. E. Olson, V. D. Rodríguez, W. Wu, M. Pieksma, and N. Watanabe, Phys. Rev. A **54**, 1394 (1996).
[11] W. Wu, K. L. Wong, R. Ali, C. Y. Chen, C. L. Cocke, V. Frone, J. P. Giese, M. Raphaelian, B. Walch, R. Dörner, V. Mergel, H. Schmidt-Böcking, and W. E. Meyerhof, Phys. Rev. Lett. **72**, 3170 (1994).
[12] R. Dörner, V. Mergel, R. Ali, U. Buck, C. L. Cocke, K. Froschauer, O. Jagutzki, S. Lencinas, W. E. Meyerhof, S. Nüttgens, R. E. Olson, H. Schmidt-Böcking, L. Spielberger, K. Tökesi, J. Ullrich, M. Unverzagt, and W. Wu, Phys. Rev. Lett. **72**, 3166 (1994).
[13] Y. D. Wang, Lokesh C. Tribedi, P. Richard, C. L. Cocke, V. D. Rodríguez, and C. D. Lin, J. Phys. B **29**, L203 (1996).
[14] Lokesh C. Tribedi, P. Richard, Y. D. Wang, C. D. Lin, and R. E. Olson, Phys. Rev. Lett. **77**, 3767 (1996).
[15] V. D. Rodríguez, Y. D. Wang, and C. D. Lin, J. Phys. B **18**, L471 (1995).
[16] V. D. Rodríguez, Y. D. Wang, and C. D. Lin, Phys. Rev. A **52**, R9 (1995).
[17] E. Krishnakumar, Bhas Bapat, F. A. Rajgara, and M. Krishnamurthy, J. Phys. B **27**, L777 (1994).
[18] S. Cheng, C. L. Cocke, E. Y. Kamber, C. C. Hsu, and S. L. Varghese, Phys. Rev. A **42**, 214 (1990).
[19] E. Krishnakumar and F. A. Rajgara, J. Phys. B **26**, 4155 (1993).
[20] T. Vajnai, A. D. Gaus, J. A. Brand, W. Htwe, D. H. Madison, R. E. Olson, J. L. Peacher, and M. Schulz, Phys. Rev. Lett. **74**, 3588 (1995).
[21] R. Dörner, V. Mergel, L. Zhaoyuan, J. Ulrich, L. Spielberger, R. E. Olson, and H. Schmidt-Böcking, J. Phys. B **28**, 435 (1995).